Optics & Laser Technology 152 (2022) 108079

Contents lists available at ScienceDirect

Optics and Laser Technology

journal homepage: www.elsevier.com/locate/optlastec

A class of vectorial pseudo-Schell model sources with structured coherence and polarization

Rosario Martínez-Herrero [a,*], Gemma Piquero [a], Massimo Santarsiero [b], Franco Gori [b], Juan Carlos González de Sande [c]

[a] Departamento de Óptica, Universidad Complutense de Madrid, Madrid 28040, Spain
[b] Dipartimento di Ingegneria Industriale, Elettronica e Meccanica, Università Roma Tre, Via V. Volterra 62, Rome 00146, Italy
[c] ETSIS de Telecomunicación, Universidad Politécnica de Madrid, Campus Sur, Madrid 28031, Spain

ARTICLE INFO

Keywords:
Coherence
Polarization
Propagation
Degree of coherence
Structured light

ABSTRACT

Scalar pseudo-Schell model sources present a degree of coherence depending only on the difference between the radial coordinates of the two considered points. Here we study a class of sources of this kind, but endowed with a vectorial nature. Such sources, as well as the beams they radiate, present structured coherence and polarization features. It is shown that the polarization pattern and the degree of polarization are not uniform across the beam section but remain invariant upon paraxial propagation. Different characteristics of the source and the radiated beam can be obtained by changing the source parameters. Some synthesis procedures are also proposed.

1. Introduction

The proposal of new types of light sources with structured coherence is a subject of increasing recent research in the literature, for both scalar [1–17] and vector sources [18–30]. The interest for the beams they radiate lies in the peculiar properties that they may present, which find application in several fields. Just to quote some, we recall self-focusing, particle trapping, propagation through turbulent media, and imaging [24,31–43].

A recently introduced example of structured sources in the scalar realm are the so-called pseudo-Schell model (PSM) sources [13,14], which present coherence characteristics that only depend on the difference of the distances of two points from the source center, i.e., on the difference of their radial coordinates. It has been shown that these beams present self-focusing effect and may find application in particle trapping [14,15].

In this work we focus our attention onto sources that behave as scalar pseudo-Schell model sources as far as the radial coordinate is concerned, but are endowed with a vectorial nature, presenting position-dependent polarization properties. We call them vectorial pseudo-Schell model (VPSM) sources. In particular, we will study the coherence and polarization features of a class of such sources and of the beams they radiate in the paraxial regime. The free parameters of the sources of this class allow one to conceive a wide variety of beams with structured coherence and polarization which present several interesting properties.

For example, the degree of polarization may change across the source plane, from totally polarized to completely unpolarized, and also the state of polarization can be not uniform across the source. In any case, the transverse patterns of the polarization state and of the polarization degree remain invariant during propagation. Furthermore, both the intensity profile and the coherence depend on the chosen parameters of the source and change during propagation but, in any case, the intensity has a null at the source center, which is always preserved in the propagated beam. This gives rise to a dark hollow beam with structured coherence and polarization. The above features could be applied, for example, for measuring size and morphology of carbon nanotubes [44], for observing the spin Hall effect [45], or in polarimetry [46,47].

We also show a technique for the experimental synthesis of the proposed vector sources. The technique stems on their representation as the incoherent superposition of perfectly coherent and perfectly polarized vector fields.

This paper is structured as follows. This Section constitutes the Introduction while Section 2 is devoted to the description of the tools used to describe the source and to study their characteristics. In Section 3, the passage from a scalar case to a vectorial class is described. In Section 4, the proposed vectorial pseudo-Schell model source is

* Corresponding author.
E-mail addresses: r.m-h@fisucm.es (R. Martínez-Herrero), piquero@ucm.es (G. Piquero), massimo.santarsiero@uniroma3.it (M. Santarsiero), franco.gori@uniroma3.it (F. Gori), juancarlos.gonzalez@upm.es (J.C. González de Sande).

https://doi.org/10.1016/j.optlastec.2022.108079
Received 21 December 2021; Received in revised form 16 February 2022; Accepted 15 March 2022
Available online 25 March 2022

introduced and their characteristics in the source plane are analyzed in detail. Afterwards, the paraxial propagation and the main features of the radiated beam are described in Section 5. Synthesis procedures are described in Section 6 and, finally, the main results are summarized in Section 7.

2. Preliminaries

Within the framework of the paraxial approximation, one can account for the complete set of space-frequency correlation functions at two typical points ($\boldsymbol{r}_1$ and $\boldsymbol{r}_2$) of a planar source by using the cross-spectral density (CSD) matrix [48], $\widehat{W}(\boldsymbol{r}_1, \boldsymbol{r}_2)$, whose elements are defined as

$$W_{\gamma\zeta}\left(\boldsymbol{r}_1,\boldsymbol{r}_2\right) = \left\langle E_\gamma^*\left(\boldsymbol{r}_1\right)E_\zeta\left(\boldsymbol{r}_2\right)\right\rangle, \tag{1}$$

(with $\gamma,\zeta = x,y$) where E_γ is the γ-component of the electric field, the brackets denote ensemble average, and the dependence on the temporal frequency has been omitted for brevity. The analogous quantity in the space–time domain is the so-called beam coherence-polarization (BCP) matrix [49]. It should be kept in mind that, in order for a 2×2 matrix to represent the CSD matrix of a physically realizable source, the non-negativity condition has to be met [49,48,50,51].

The local properties of the source are given by the CSD matrix evaluated for $\boldsymbol{r}_1 = \boldsymbol{r}_2 = \boldsymbol{r}$, namely, $\widehat{W}(\boldsymbol{r},\boldsymbol{r})$. In particular, the optical intensity of the source and its degree of polarization at the point $\boldsymbol{r}$ turn out to be [48]

$$I(\boldsymbol{r}) = S_0(\boldsymbol{r}) = \mathrm{Tr}[\widehat{W}(\boldsymbol{r},\boldsymbol{r})] \tag{2}$$

and

$$P\left(\boldsymbol{r}\right) = \sqrt{1-\frac{4\,\mathrm{Det}[\widehat{W}(\boldsymbol{r},\boldsymbol{r})]}{\{\mathrm{Tr}[\widehat{W}(\boldsymbol{r},\boldsymbol{r})]\}^2}}, \tag{3}$$

respectively, where Det stands for determinant and Tr for trace.

The local state of polarization can be described by the Stokes parameters of the field and can be calculated starting from the values of the elements of the CSD matrix as follows [52,53]:

$$\mathbf{S}\left(\boldsymbol{r}\right) = \begin{bmatrix} S_0(\boldsymbol{r}) \\ S_1(\boldsymbol{r}) \\ S_2(\boldsymbol{r}) \\ S_3(\boldsymbol{r}) \end{bmatrix} = \begin{bmatrix} W_{xx}\left(\boldsymbol{r},\boldsymbol{r}\right) + W_{yy}\left(\boldsymbol{r},\boldsymbol{r}\right) \\ W_{xx}\left(\boldsymbol{r},\boldsymbol{r}\right) - W_{yy}\left(\boldsymbol{r},\boldsymbol{r}\right) \\ 2\,\mathrm{Re}\left[W_{yx}\left(\boldsymbol{r},\boldsymbol{r}\right)\right] \\ 2\,\mathrm{Im}\left[W_{yx}\left(\boldsymbol{r},\boldsymbol{r}\right)\right] \end{bmatrix}, \tag{4}$$

with Re and Im denoting the real and the imaginary part, respectively. We will refer to the state of polarization of the polarized part as the one calculated from $S_1(\boldsymbol{r}), S_2(\boldsymbol{r}), S_3(\boldsymbol{r})$ and considering $S_{0,TP}^2(\boldsymbol{r}) = S_1^2(\boldsymbol{r}) + S_2^2(\boldsymbol{r}) + S_3^2(\boldsymbol{r})$ instead of S_0 defined in Eq. (4).

On the other hand, several scalar quantities have been proposed to give account of the coherence properties of the source [48,54–58]. All of them, of course, can be evaluated from the expression of the CSD matrix of the source but, for brevity, we shall limit ourselves to consider three of them.

The first one follows from a direct extension of the definition used for scalar fields and is related to the visibility of the fringes produced by the field in a Young interferometer [53]. For a vector field, two systems of fringes will be superposed due to the x and the y components. Being orthogonally polarized their intensities are simply summed up. This lead to define an *equivalent* DoC, introduced by Wolf [50,59,60] as

$$\left|\mu_{\mathrm{W}}\left(\boldsymbol{r}_1,\boldsymbol{r}_2\right)\right|^2 = \frac{|\mathrm{Tr}[\widehat{W}(\boldsymbol{r}_1,\boldsymbol{r}_2)]\,|^2}{I(\boldsymbol{r}_1)I(\boldsymbol{r}_2)}. \tag{5}$$

The second one is the so called *electromagnetic* DoC. It is defined by [54,55]

$$\mu_{\mathscr{E}}^2\left(\boldsymbol{r}_1,\boldsymbol{r}_2\right) = \frac{\mathrm{Tr}[\widehat{W}^\dagger(\boldsymbol{r}_1,\boldsymbol{r}_2)\widehat{W}(\boldsymbol{r}_1,\boldsymbol{r}_2)]}{I(\boldsymbol{r}_1)I(\boldsymbol{r}_2)}, \tag{6}$$

with the dagger denoting hermitian conjugation, and gives a global measure of the correlation among all the components of the field at the two points.

The third one is the *maximum-visibility* DoC [56,57], which can be expressed by

$$\mu_{\mathscr{V}}^2\left(\boldsymbol{r}_1,\boldsymbol{r}_2\right) = \frac{\mathrm{Tr}[\widehat{W}^\dagger(\boldsymbol{r}_1,\boldsymbol{r}_2)\widehat{W}(\boldsymbol{r}_1,\boldsymbol{r}_2)] + 2|\mathrm{Det}[\widehat{W}(\boldsymbol{r}_1,\boldsymbol{r}_2)]\,|}{I(\boldsymbol{r}_1)I(\boldsymbol{r}_2)}. \tag{7}$$

It quantifies the maximum fringe visibility that can be obtained in a Young experiment on modifying the interfering fields by means of unitary transformations [56,57].

Note that the equivalent DoC is enough if one is only interested in fringe visibility, but it does not give any information about different field components correlation. The complete information is contained in the BCP matrix [49]. If, however, one wants to account for the various correlations with a single quantity, the electromagnetic degree of coherence (DoC) or the maximum-visibility DoC can be used. The latter can be directly measured in the laboratory using a Simon-Mukunda device [61,62]. Once the maximum-visibility DoC is known the electromagnetic DoC is easily derived. The relationship between two of these parameters or one of them with other parameters proposed as DoC has been debated [58,61,63].

Assuming paraxial conditions, the propagated CSD matrix can be calculated by means of the Fresnel diffraction integral [53]. Considering the propagation direction mainly along the z axis of a suitable reference frame, the propagated CSD matrix can be written as [53]

$$\begin{aligned}\widehat{W}_z(\mathbf{R}_1,\mathbf{R}_2) = {} & \frac{1}{\lambda^2 z^2}\iint \widehat{W}(\mathbf{r}_1,\mathbf{r}_2) \\ & \times\exp\left[-\frac{ik}{2z}\left(|\mathbf{R}_1-\mathbf{r}_1|^2+|\mathbf{R}_2-\mathbf{r}_2|^2\right)\right]\mathrm{d}^2\mathbf{r}_1\mathrm{d}^2\mathbf{r}_2,\end{aligned} \tag{8}$$

where $\lambda = 2\pi/k$ is the wavelength and $\mathbf{R}_j = (R_j,\vartheta_j)$, with $j = 1,2$, are two typical position vectors in the plane $z =$ constant.

3. From the scalar to the vectorial case

Let us consider a scalar source of the pseudo-Schell model type, i.e. a source whose CSD has the form [13,14]

$$W(\boldsymbol{r}_1,\boldsymbol{r}_2) = \tau^*(\boldsymbol{r}_1)\,\tau(\boldsymbol{r}_2)g(r_2-r_1), \tag{9}$$

where τ accounts for some (amplitude and/or phase) modulation across the source plane and g is proportional to the (scalar) DoC

$$\mu\left(\boldsymbol{r}_1,\boldsymbol{r}_2\right) = \frac{W(\boldsymbol{r}_1,\boldsymbol{r}_2)}{\sqrt{W(\boldsymbol{r}_1,\boldsymbol{r}_1)W(\boldsymbol{r}_2,\boldsymbol{r}_2)}} = g\left(r_2-r_1\right)\exp\left\{i\left[\phi\left(\boldsymbol{r}_2\right)-\phi\left(\boldsymbol{r}_1\right)\right]\right\}, \tag{10}$$

ϕ being the phase of τ.

Let us also assume the function τ to be of the form of a TEM_{10} Hermite-Gauss mode

$$\tau\left(\boldsymbol{r}\right) = \tau\left(\boldsymbol{x},\boldsymbol{y}\right) = \boldsymbol{A}\frac{\boldsymbol{x}}{\boldsymbol{w_0}}\exp\left(-\frac{\boldsymbol{x^2}+\boldsymbol{y^2}}{\boldsymbol{w_0^2}}\right), \tag{11}$$

at its waist. Here, w_0 is the waist spot-size and A is a proportionality factor. Alternativey, the same function can be expressed with polar coordinates as

$$\tau(r,\theta) = \tau_r(r)\cos\theta, \tag{12}$$

with

$$\tau_r\left(r\right) = A\,\frac{r}{w_0}\exp\left(-\frac{r^2}{w_0^2}\right). \tag{13}$$

This is the expression in which we are mostly interested. As for g we assume it to be Gaussian, too

$$g\left(r_2 - r_1\right) = \exp\left[-\frac{\left(r_2 - r_1\right)^2}{\delta^2}\right]. \tag{14}$$

Most of the properties derived from the sources proposed in this paper are independent of this particular choice. Note that while w_0 is related to the width of the intensity, δ accounts for a statistical process and determines the extent of the region in which high correlation of the field components occurs. The overall CSD across the waist plane is then

$$W(r_1,\theta_1;r_2,\theta_2) = \frac{|A|^2 r_1 r_2 \cos\theta_1\cos\theta_2}{w_0^2}\exp\left(-\frac{r_1^2+r_2^2}{w_0^2}\right) \times\exp\left[-\frac{\left(r_2-r_1\right)^2}{\delta^2}\right]. \tag{15}$$

The presence of an angular dependence entails that the intensity distribution is not circularly symmetric. In fact we have

$$I\left(r,\theta\right) = W\left(r,\theta;r,\theta\right) = \frac{|A|^2 r^2\cos^2\theta}{w_0^2}\exp\left(-\frac{2r^2}{w_0^2}\right), \tag{16}$$

which depicts the well-known coffee grain. On the other hand, the modulus of the DoC for any pair of points, excluding the origin, is expressed by the last Gaussian of Eq. (15). It will be noticed that using Eqs. (9) and (15) the CSD can be written in the product form

$$W(\boldsymbol{r}_1,\boldsymbol{r}_2) = W_{\mathrm{PS}}(r_1,r_2)\,\Theta(\theta_1,\theta_2), \tag{17}$$

where

$$\Theta(\theta_1,\theta_2) = \cos\theta_1\cos\theta_2, \tag{18}$$

and

$$W_{\mathrm{PS}}\left(r_1,r_2\right) = \frac{|A|^2 r_1 r_2}{w_0^2}\exp\left(-\frac{r_1^2+r_2^2}{w_0^2}\right)\exp\left[-\frac{\left(r_2-r_1\right)^2}{\delta^2}\right], \tag{19}$$

which is a particular case of pseudo-Schell model source.

An advantage of this separability is that this property remains invariant in propagation, i.e., the CSD of the propagated field can be expressed as a product of two functions, one of them that depends only on the radial coordinates and the other one on the angular variables. In addition, the integration over the angular variables of the $\cos\theta$ terms will produce J_1 Bessel functions, which simplifies the study of paraxial propagation.

When the vectorial aspects of the electromagnetic field are detectable a vectorial version of the CSD is needed. The single CSD function is then replaced by a set of correlation functions for each possible pair of field components given in Eq. (1). When for the x component of the field the one giving rise to Eq. (18) is selected, and for the y component the same field is adopted but angularly shifted by the angle α, and further assuming partial correlation between the two components, the resulting CSD matrix can be written as

$$\widehat{W}(\boldsymbol{r}_1,\boldsymbol{r}_2) = W_{\mathrm{PS}}(r_1,r_2)\widehat{\Theta}(\theta_1,\theta_2). \tag{20}$$

where $W_{\mathrm{PS}}(r_1,r_2)$ is a scalar CSD of the pseudo-Schell model type and $\widehat{\Theta}$ has the form

$$\widehat{\Theta}\left(\theta_1,\theta_2\right) = \begin{bmatrix} \cos\theta_1\cos\theta_2 & b\cos\theta_1\cos(\theta_2-\alpha) \\ b^*\cos(\theta_1-\alpha)\cos\theta_2 & \cos(\theta_1-\alpha)\cos(\theta_2-\alpha), \end{bmatrix}. \tag{21}$$

Here, b expresses the correlation between the two components. The CSD matrix defined by Eqs. (19)–(21) satisfies the non-negativeness condition whenever $|b|\leqslant 1$.

4. Nonuniformly polarized VPSM with propagation invariant characteristics

In this work, the broad class of partially coherent vector sources introduced in the previous section is investigated. The form of the CSD matrix is that defined in Eqs. (19)–(21). The radial dependence of the degrees of coherence pertinent to W_{PS} can be varied on changing the function $g(r)$ (see Eq. (14)), thus obtaining a wider variety of pseudo-Schell model sources, but all of them present some common characteristics, as it was shown for the scalar case [13,14]. On the other hand, the function $\tau_r(r)$ affects the intensity distribution across the source plane. Conversely, the degree of polarization and the polarization state of the polarized part are independent of the particular form of $W_{\mathrm{PS}}(r_1,r_2)$.

4.1. Characteristics at the source plane

The characteristics of this VPSM source, i.e., the intensity, the state and degree of polarization, and the degrees of coherence across the source plane can be obtained by substituting the proposed CSD matrix into Eqs. (2)–(7).

In particular, the intensity across the source turns out to be

$$I(\mathbf{r}) = |\tau_r(r)|^2\left[\cos^2\left(\theta\right) + \cos^2\left(\theta-\alpha\right)\right]. \tag{22}$$

It follows that the intensity profile does not present circular symmetry, except for specific values of the source parameters. In fact, it changes from two symmetrical lobes (for $\alpha = m\pi$, with m integer) to a circularly symmetrical doughnut (for $\alpha = \pi/2 + m\pi$). Moreover, the intensity always vanishes at the center of the source. These features can be seen in Fig. 1, where the intensity profile is shown for eight values of α.

One may ask which relationship exists between the direction of the principal axes of the beam profile and α (excluding, of course, $\alpha = \pi/2 + m\pi$, in which case the intensity is circularly symmetric). To answer this question let us recall that the principal axes are those for which the widths $\sqrt{\langle x^2\rangle}$ and $\sqrt{\langle y^2\rangle}$ reach their extreme values [64,65].

If we call χ the angle formed by one of the principal axes with respect to the x axis we obtain [64,65]

$$\cot\left(2\chi\right) = \frac{\langle x^2\rangle - \langle y^2\rangle}{2\,\langle xy\rangle}, \tag{23}$$

which in our case turns out to be

$$\cot(2\chi) = \cot(\alpha). \tag{24}$$

It is interesting to note that the orientation of these principal axes (which is undetermined for $\alpha = \pi/2 + m\pi$, as was expected) is independent of the choice of $\tau_r(r)$ and $g(r)$. A jump from $\chi = \pi/4$ to $\chi = -\pi/4$ occurs for $\alpha = \pi/2 + m\pi$. The degree of polarization can be evaluated at each point of the source plane as (see Eqs. (2)–(7)

$$P(\mathbf{r}) = \frac{\sqrt{\left[\cos^2(\theta)-\cos^2(\theta-\alpha)\right]^2 + 4\left|b\right|^2\cos^2\left(\theta\right)\cos^2\left(\theta-\alpha\right)}}{\cos^2(\theta)+\cos^2(\theta-\alpha)}, \tag{25}$$

and turns out to be independent of the particular form of $W_{\mathrm{PS}}(r_1,r_2)$. A significant feature of the degree of polarization is that it is not uniform in the source plane, as it can be seen in Fig. 2. In particular, it is the same along any selected radial line but varies with the angular coordinate, ranging from a minimum value, which depends on the value of b, to 1.

Some values of the source parameters give rise to a uniform degree of polarization. For example, for $|b| = 1$, the degree of polarization is unitary throughout the whole source plane, although the polarization state may vary from point to point. Finally, it can be seen that for

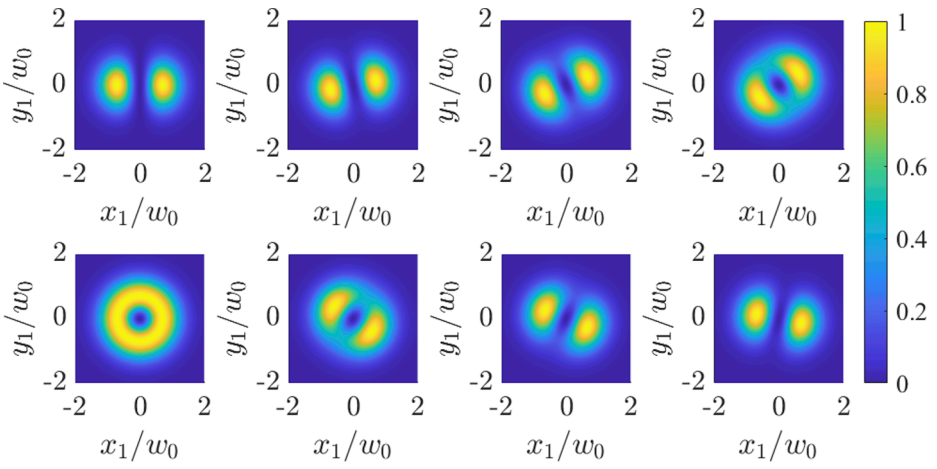

Fig. 1. Intensity (normalized to its maximum) at the source plane with the source parameters $\delta = 0.25w_0$ and $b = 0.5$, for $\alpha = 0$, $\alpha = \pi/8$, $\alpha = \pi/4$, $\alpha = 3\pi/8$, $\alpha = \pi/2$, $\alpha = 5\pi/8$, $\alpha = 3\pi/4$ and $\alpha = 7\pi/8$, from left to right and top to bottom.

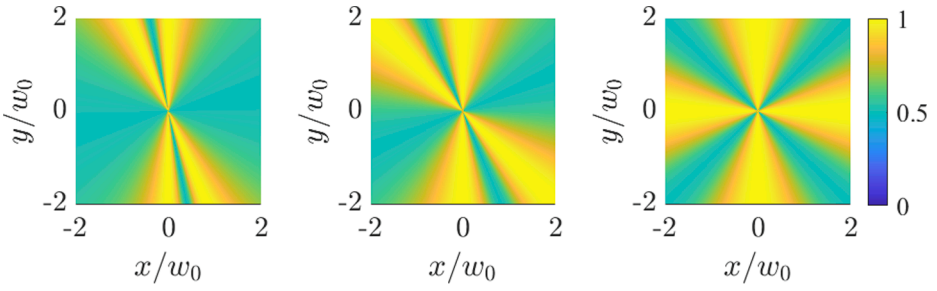

Fig. 2. Degree of polarization at the source plane with the source parameters $\delta = 0.25w_0$ and $b = 0.5$ for $\alpha = \pi/8$ (left), $\alpha = \pi/4$ (center), and $\alpha = \pi/2$ (right). Note that for $\alpha = 0$, then $P(\mathbf{r}) = |b|$ in the whole source plane.

α=0 the degree of polarization is $P(\mathbf{r}) = |b|$ for the entire source plane.

The Stokes parameters are evaluated, from Eq. (4), as

$$\begin{bmatrix} S_0(r,\theta) \\ S_1(r,\theta) \\ S_2(r,\theta) \\ S_3(r,\theta) \end{bmatrix} |\tau_r(r)|^2 \begin{bmatrix} \cos^2(\theta) + \cos^2(\theta-\alpha) \\ \cos^2(\theta) - \cos^2(\theta-\alpha) \\ 2\,\mathrm{Re}[b]\cos(\theta)\cos(\theta-\alpha) \\ 2\,\mathrm{Im}[b]\cos(\theta)\cos(\theta-\alpha) \end{bmatrix}. \tag{26}$$

It follows from this expression that the polarized part of the source has, in general, a nonuniform polarization pattern. For real values of the parameter b, the polarization state of the polarized part is always linear, but its azimuth varies as a function of the values of the source parameters. The polarization state of the polarized part is shown, together with the intensity map, in Fig. 3 for $\delta = 0.25w_0, \alpha = \pi/4$, and two different values of b (namely, $b = 0.5$ and $b = 0.5\mathrm{i}$). It can be seen that different polarization patterns are obtained with the same degree of polarization. Regarding the coherence properties, the equivalent DoC is easily evaluated as (see Eq. (4),

$$\mu_W^2\left(\boldsymbol{r}_1, \boldsymbol{r}_2\right) = N_W\left(\theta_1, \theta_2\right) \exp\left[-\frac{2(r_1 - r_2)^2}{\delta^2}\right], \tag{27}$$

where

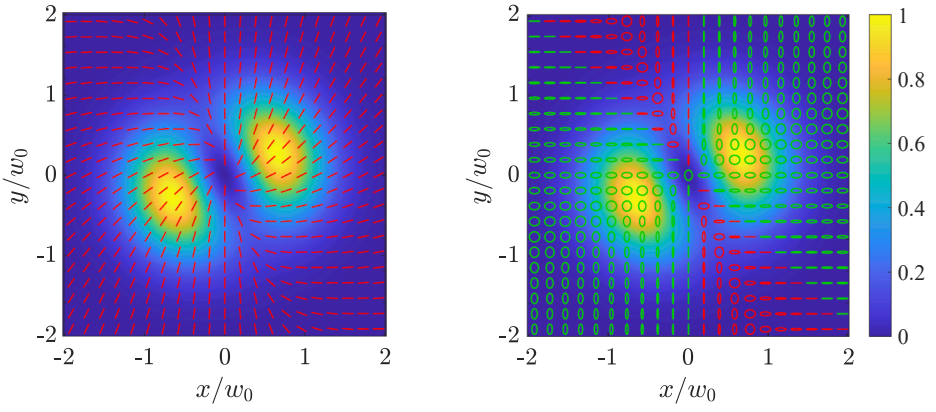

Fig. 3. Ellipses of polarization of the polarized part at the source plane (superimposed to the intensity map) with the source parameters $\delta = 0.25w_0$ and $\alpha = \pi/4$ for $b = 0.5$ (left), and $b = 0.5\mathrm{i}$ (right). Handedness is codified in color: red for right-handed ellipses (and linear polarization) and green for left-handed polarization.

$$N_W\left(\theta_1,\theta_2\right)=\frac{\left[\cos\theta_1\cos\theta_2+\cos(\theta_1-\alpha)\cos(\theta_2-\alpha)\right]^2}{\left[\cos^2(\theta_1)+\cos^2(\theta_1-\alpha)\right]\left[\cos^2(\theta_2)+\cos^2(\theta_2-\alpha)\right]}. \tag{28}$$

A few examples of the corresponding DoC vs θ_1 for $r_1 = r_2$, with $\alpha=\pi/6$ and several values of θ_2, are shown in Fig. 4. The electromagnetic DoC is evaluated as (see Eq. (4),

$$\mu^2_{\mathscr{E}}\left(\boldsymbol{r}_1,\boldsymbol{r}_2\right)=N_{\mathscr{E}}\left(\theta_1,\theta_2\right)\exp\left[-\frac{2(r_1-r_2)^2}{\delta^2}\right], \tag{29}$$

where the function $N_{\mathscr{E}}(\theta_1,\theta_2)$ is defined as

$$\begin{aligned}N_{\mathscr{E}}(\theta_1,\theta_2)=&\left\{\cos^2(\theta_1)\cos^2(\theta_2)+\cos^2(\theta_1-\alpha)\cos^2(\theta_2-\alpha)\right.\\&\left.+|b|^2\left[\cos^2(\theta_1)\cos^2(\theta_2-\alpha)+\cos^2(\theta_2)\cos^2(\theta_1-\alpha)\right]\right\}\\&\times\left\{\left[\cos^2(\theta_1)+\cos^2(\theta_1-\alpha)\right]\left[\cos^2(\theta_2)+\cos^2(\theta_2-\alpha)\right]\right\}^{-1}.\end{aligned} \tag{30}$$

Fig. 5 shows the behaviour of the electromagnetic DoC in the source plane for the source parameters $\delta=0.25w_0, \alpha=\pi/4$, and $b=0.5$. In these plots the DoC is evaluated with respect to a point denoted by a red spot having radial coordinate r_2 and several values of θ_2. It can be noted that its maximum value does not reach 1, in general, even if it is evaluated at the same point. This is a general property of the electromagnetic DoC because it gives a measure of the correlations among all the field components [54], and is unitary for $\boldsymbol{r}_1=\boldsymbol{r}_2$ only if the field is also perfectly polarized at that point.

The angular behaviour of $\mu^2_{\mathscr{E}}$ on a circle of radius $r_1=r_2$ is shown in Fig. 6 for the same angular positions θ_2 as in Fig. 5. Since the electromagnetic DoC depends on the squared sinusoidal functions of the angular variables, it is periodic with period π for both angular variables, that is, $N_{\mathscr{E}}(\theta_1,\theta_2)=N_{\mathscr{E}}(\theta_1+m\pi,\theta_2)=N_{\mathscr{E}}(\theta_1,\theta_2+m\pi)$. It can be noted that only the curve corresponding to $\theta_2=\pi/2$ reaches a maximum equal to one. This happens, in fact, at a point where the field is perfectly polarized because one of the field components vanishes there.

The maximum-visibility DoC (see Eq. (7)) takes the following expression:

$$\mu^2_{\mathscr{V}}\left(\boldsymbol{r}_1,\boldsymbol{r}_2\right)=N_{\mathscr{V}}\left(\theta_1,\theta_2\right)\exp\left[-\frac{2(r_1-r_2)^2}{\delta^2}\right], \tag{31}$$

where the function $N_{\mathscr{V}}(\theta_1,\theta_2)$ is

$$\begin{aligned}N_{\mathscr{V}}(\theta_1,\theta_2)=&\quad N_{\mathscr{E}}(\theta_1,\theta_2)\\&+\frac{2\left|\left(1-|b|^2\right)\cos\left(\theta_1\right)\cos\left(\theta_2\right)\cos\left(\theta_1-\alpha\right)\cos\left(\theta_2-\alpha\right)\right|}{\left[\cos^2\left(\theta_1\right)+\cos^2\left(\theta_1-\alpha\right)\right]\left[\cos^2\left(\theta_2\right)+\cos^2\left(\theta_2-\alpha\right)\right]}.\end{aligned} \tag{32}$$

The behavior of $\mu^2_{\mathscr{V}}$ is shown in Fig. 7. Note that, unlike the eletromagnetic DoC, it always satisfies $\mu^2_{\mathscr{V}}(\boldsymbol{r},\boldsymbol{r})=1$, regardless of the values of the source parameters. This is due to the fact the maximum-visibility DoC, evaluated for $\boldsymbol{r}_1=\boldsymbol{r}_2$, measures the visibility of the fringes that can be obtained from the interference of a field with itself, and must be unitary independently of the polarization state of the field.

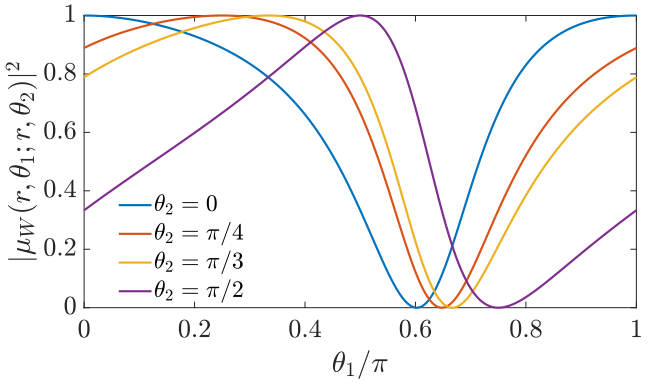

Fig. 4. Plots of equivalent DoC for $\alpha=\pi/4$.

Fig. 8 shows the behavior of the maximum-visibility DoC for points on a circle of radius $r_1=r_2$ with respect to a point on that circle with various values of the angular variable θ_2. In this case a maximum equal to 1 is always obtained, at least for $\theta_1=\theta_2$. Moreover, even in this case the angular dependence is periodic with respect the angular variables with period π, so that any pair of diametrically opposite points on the same concentric circle presents complete coherence. Moreover, depending on the value of the parameter α, there may be more pairs of fully coherent points.

5. Paraxial propagation of the radiated field

The properties of the field radiated from the source in paraxial conditions can be studied by inserting the CSD matrix given by Eq. (20) into the Fresnel diffraction integral of Eq. (8). Integrating over the angular variables, the following propagated CSD matrix is obtained:

$$\widehat{W}(\mathbf{R}_1,\mathbf{R}_2,z)=f(R_1,R_2,z)\,\widehat{\Theta}\,(\vartheta_1,\vartheta_2), \tag{33}$$

where $\widehat{\Theta}\,(\vartheta_1,\vartheta_2)$ is the same as in Eq. (21). With the functions $\tau_r(r)$ and $g(r)$ given by Eqs. (13) and (14), respectively, the auxiliary function $f(R_1,R_2,z)$ takes the form

$$\begin{aligned}f(R_1,R_2,z)=&|A|^2\frac{k^2}{z^2}\exp\left[-\frac{\mathrm{i}k}{2z}\left(R_1^2-R_2^2\right)\right]\\&\times\int\int r_1^2r_2^2\exp\left[-\frac{(r_1-r_2)^2}{\delta^2}\right]\exp\left[-\frac{ik}{2z}\left(\mathrm{r}_1^2-\mathrm{r}_2^2\right)\right]\\&\times\exp\left[-\frac{\mathrm{r}_1^2+\mathrm{r}_2^2}{\mathrm{w}_0^2}\right]\mathrm{J}_1\left(\frac{kr_1\mathrm{R}_1}{\mathrm{z}}\right)\mathrm{J}_1\left(\frac{kr_2\mathrm{R}_2}{\mathrm{z}}\right)\mathrm{d}r_1\mathrm{d}r_2,\end{aligned} \tag{34}$$

$J_n(\cdot)$ being the Bessel function of the first kind and order n [66].

As can be seen from Eq. (33), the polarization characteristics given by $\widehat{\Theta}\,(\vartheta_1,\vartheta_2)$ are identical to those of the source plane, i.e., the same transverse patterns of either the state and the degree of polarization are obtained at any z-plane. On the contrary, the intensity of the beam evolves as

$$I(\mathbf{r})=|f(R,R,z)|^2\left[\cos^2(\theta)+\cos^2(\theta-\alpha)\right], \tag{35}$$

still retaining the same angular dependence as at the source plane.

An interesting feature of the propagated intensity, derived from the expression in Eq. (34), is that it vanishes along the entire z-axis. Also, that the orientation of the principal axes does not change during propagation because it depends on the parameter α but not on the particular choice of the scalar CSD $W_{\mathrm{PS}}(r_1,r_2)$.

For the choice $\alpha=\pi/2$, i.e., when the intensity profile is circularly symmetric, the evolution of the propagating intensity profile, shown in Fig. 9, is the same as in the scalar case for a vortex Gaussian pseudo-Schell source with topological charge equal to 1 (see Figs. 7–10 in Ref. [13]). In this figure, the propagation distance is expressed in terms of the Rayleigh distance $z_R=kw_0^2/2$. The profile in the source plane corresponds to the shape of a Laguerre–Gaussian coherent beam of zero order and topological charge equal to 1. Unlike the usual partially coherent hollow beams of the Schell-model type [67–69], the null at the center of the beam is maintained in propagation. Moreover, a ring of higher intensity and smaller radius appears in propagation. It can be observed that the maximum intensity is reached after a certain propagation distance. This can be considered as a self focusing effect of this kind of sources.

The evolution of the intensity profile for a noncircularly symmetric case is shown in Fig. 10, where the parameters δ and b are the same as in Fig. 1, but $\alpha=\pi/4$. It can be noted that also in this case the maximum

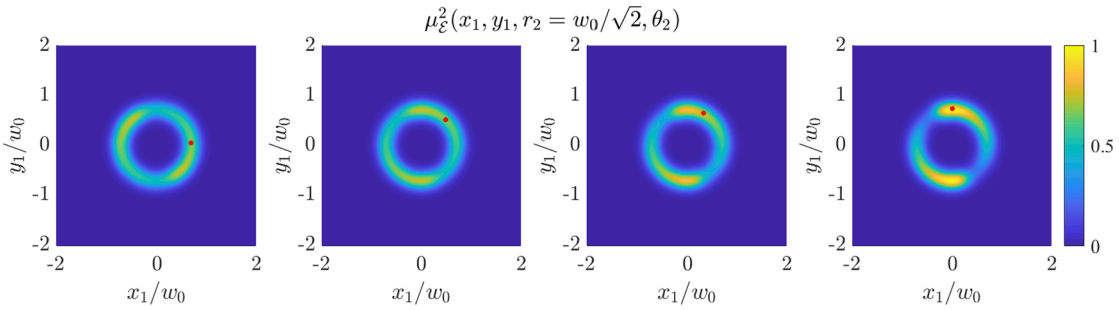

Fig. 5. Electromagnetic DoC relative to a point (red spot) located on the circle where the maximum intensity is reached for angles $\theta_2 = 0,\ \pi/4, \pi/3$, and $\pi/2$, respectively, from left to right (source parameters $\delta = 0.25w_0, \alpha = \pi/4$, and $b = 0.5$).

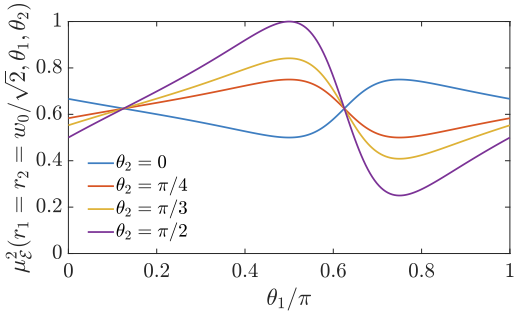

Fig. 6. Electromagnetic DoC relative to a point located on a circle of radius r_2 and angles $\theta_2 = 0,\ \pi/4, \pi/3$, and $\pi/2$, respectively, for points $\boldsymbol{r}_1$ on the same circle (source parameters $\delta = 0.25w_0, \alpha = \pi/4$, and $b = 0.5$).

intensity is not reached at the source plane (see the colorbar scale) but after a certain propagation distance.

As regards the degrees of coherence, the following relations can be obtained

$$\frac{\mu^2_{\mathscr{E}}(\boldsymbol{R}_1, \boldsymbol{R}_2, z)}{\mu^2_{\mathscr{E}}(\boldsymbol{r}_1, \boldsymbol{r}_2, z = 0)} = \frac{W_{PS}(r_1, r_1)\, W_{PS}(r_2, r_2)\, |f(R_1, R_2, z)|^2}{f(R_1, R_1, z) f(R_2, R_2, z)\, |W_{PS}(r_1, r_2)|^2}. \tag{36}$$

From this result it can be observed that the angular dependence of the electromagnetic DoC remains invariant in propagation, that is

$$\mu^2_{\mathscr{E}}(R, \vartheta_1, R, \vartheta_2, z) = \mu^2_{\mathscr{E}}(r, \theta_1, r, \theta_2, z = 0). \tag{37}$$

After some tedious but straightforward algebra, similar result is obtained for the maximum-visibility DoC

$$\mu^2_{\mathscr{V}}(R, \vartheta_1, R, \vartheta_2, z) = \mu^2_{\mathscr{V}}(r, \theta_1, r, \theta_2, z = 0). \tag{38}$$

These two results mean that both the electromagnetic DoC and the maximum-visibility DoC, measured over a ring concentric to the source, remain invariant in propagation.

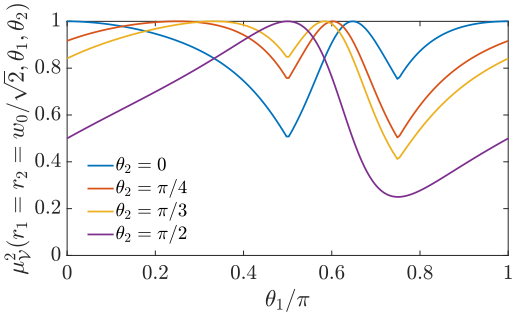

Fig. 8. Maximum-visibility DoC relative to a point located on a circle of radius r_2 and angles $\theta_2 = 0,\ \pi/4, \pi/3$, and $\pi/2$, respectively, for points $\boldsymbol{r}_1$ on the same circle (source parameters $\delta = 0.25w_0, \alpha = \pi/4$, and $b = 0.5$).

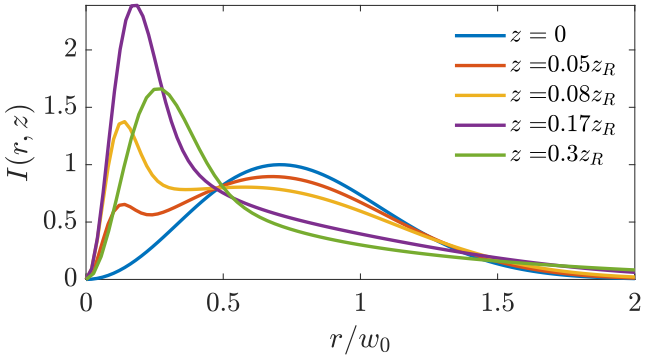

Fig. 9. Intensity profile for $\delta = w_0/5$ at several propagation distances (with $\alpha = \pi/2$, for which the intensity is circularly symmetric). The intensity profile is independent of parameter b.

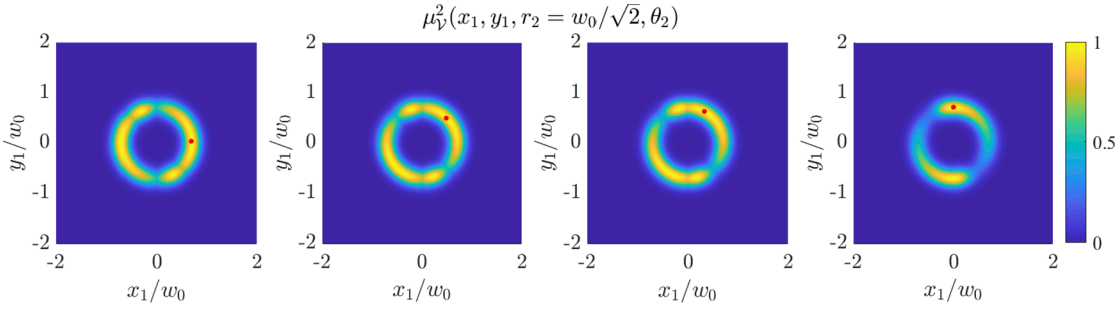

Fig. 7. Maximum-visibility DoC relative to a point (red spot) located on the circle where the intensity is maximum for $\delta = w_0/4$ and angles $\theta_2 = 0,\ \pi/4, \pi/3$, and $\pi/2$, respectively, from left to right (source parameters $\delta = 0.25w_0, \alpha = \pi/4$, and $b = 0.5$).

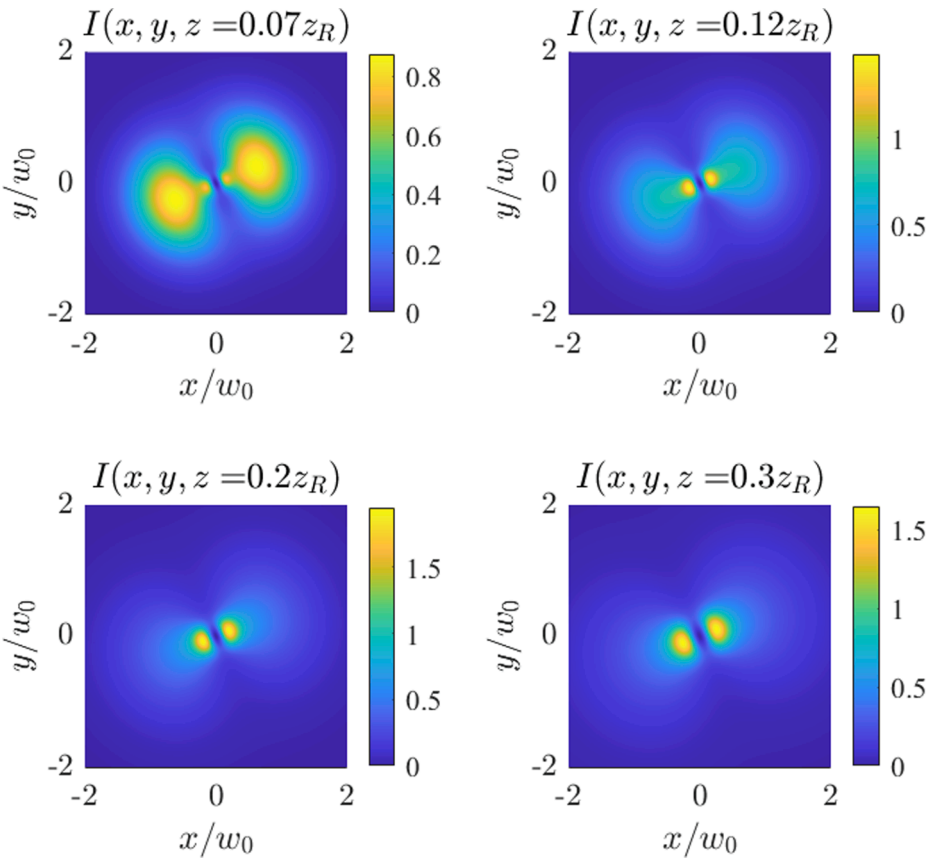

Fig. 10. Intensity maps (normalized to the maximum of the intensity at the source plane) for several propagation distances. The source parameters are $\delta = 0.25w_0$, $\alpha = \pi/4$, and $b = 0.5$.

6. Synthesis procedures

Well-known procedures for the synthesis of partially coherent sources stem on the incoherent superposition of coherent fields. This seems to be the most affordable approach when one deals with sources that are not of the Schell-model type, and has been followed for the synthesis of both scalar and vectorial sources [5,10,11,27,28,30,70–72]. The superimposed fields can be given by the so-called modes, i.e, the eigenfunctions of the homogeneous Fredholm integral equation whose kernel is the CSD function (matrix, for vector sources), and their powers by the corresponding eigenvalues [48,50,73]. Due to the mathematical properties of the CSD function, the modes are mutually orthogonal and the eigenvalues nonnegative. When the same approach is used, but with nonorthogonal coherent fields, one speaks more properly of pseudo-modes [74,51,13]. From an experimental point of view, it is often convenient to use a single laser to produce all the modes, but one at a time. The incoherent superposition of the modes is then performed by exploiting the integration time of the used detector, or summing the obtained intensity values a posteriori.

In this section we derive a pseudo-modal expansion for the CSD matrix of Eq. (20), with the functions defined in Eqs. (19)–(21), and show two possible experimental schemes for its synthesis.

Let us start from the result given in [13], pertinent to a scalar pseudo-Schell model source. In that case a pseudo-modal expansion was found, which for the CSD in Eq. (19) can be written as

$$W_{\mathrm{PS}}(r_1,r_2)=\sum_{n=0}^{\infty}\lambda_n\psi_n^*(r_1)\psi_n(r_2), \tag{39}$$

with

$$\lambda_n=\frac{I}{2^n n!}\left[1+\frac{\delta^2}{w_0^2}+\frac{\sqrt{2}\,\delta}{w_0}\left(1+\frac{\delta^2}{2w_0^2}\right)^{1/2}\right]^{-n}, \tag{40}$$

and

$$\psi_n\left(r\right)=rH_n\left(\sqrt{2\eta}\,r\right)\exp\left(-\eta r^2\right), \tag{41}$$

where $H_n(\cdot)$ is the Hermite polinomial of order n [66], and

$$\eta=\frac{1}{w_0^2}\left(1+\frac{2w_0^2}{\delta^2}\right)^{1/2}. \tag{42}$$

The matrix $\widehat{\Theta}\,(\theta_1,\theta_2)$, in turn, can be expressed in an analogous way as that pertinent to the superposition of two mutually uncorrelated perfectly polarized field, having suitable polarizations and powers. In particular, we can write

$$\widehat{\Theta}\left(\theta_1,\theta_2\right)=\sum_{j=1}^{2}a_j\,\mathbf{V}_j^{\dagger}\left(\theta_1\right)\mathbf{V}_j\left(\theta_2\right), \tag{43}$$

where the fields, written as row vectors, have the expressions

$$\begin{aligned}\mathbf{V}_1(\theta)&=\frac{1}{\sqrt{2}}\left(cos\theta\quad cos(\theta-\alpha)\,e^{i\beta}\right);\\ \mathbf{V}_2(\theta)&=\frac{1}{\sqrt{2}}\left(cos\theta\,e^{-i\beta}\quad -cos(\theta-\alpha)\right),\end{aligned} \tag{44}$$

and carry powers proportional to

$$a_1=1+|b|;\;\; a_2=1-|b|, \tag{45}$$

respectively. Parameter β denotes the phase of b.

Inserting Eqs. (39) and (43) into Eq. (20), the following expression is obtained:

$$\widehat{W}(\mathbf{r}_1,\mathbf{r}_2)=\sum_{n=0}^{\infty}\sum_{j=1}^{2}\lambda_n a_j\left[\psi_n(r_1)\mathbf{V}_j(\theta_1)\right]^{\dagger}\left[\psi_n(r_2)\mathbf{V}_j(\theta_2)\right], \tag{46}$$

which represents the pseudo-modal expansion of $\widehat{W}(\mathbf{r}_1,\mathbf{r}_2)$ we were looking for. Each mode, that is,

$$\mathbf{\Psi}_{nj}(\mathbf{r})=\psi_n(r)\mathbf{V}_j(\theta), \tag{47}$$

is a field which is fully polarized but not uniformly, except for $\alpha = m\pi$, in which case the two fields are uniformly polarized with orthogonal polarization states over the entire beam cross section.

Note that, in general, $\mathbf{V}_1(\theta)$ and $\mathbf{V}_2(\theta)$ are not orthogonal, the only exception being for $\alpha = 0$.

Fig. 11 shows the polarization patterns of the vectors $\mathbf{V}_1(\theta)$ and $\mathbf{V}_2(\theta)$ for $\alpha = \pi/4$ and two different values of β. In general, the polarization of these two fields is not uniform. When the phase of the parameter b is neither zero nor a multiple of π, i.e., $\beta \neq m\pi$, the fields $\mathbf{V}_1(\theta)$ and $\mathbf{V}_2(\theta)$ have opposite handedness (the Stokes parameter S_3 is the same but with opposite sign). For $\alpha \neq m\pi$, it is possible to find points where these two fields present orthogonal states of polarization and they obey to the condition

$$\cos^2\left(\theta\right)=\cos^2\left(\theta-\alpha\right);\quad \text{i.e.,}\quad \theta=\frac{\alpha+m\pi}{2}. \tag{48}$$

The angular dependence of the corresponding intensity is shown in Fig. 12 for several values of parameter α. Note that the two modes are weighted by constants a_1 and a_2 respectively, so that the total intensity follows the same angular dependence.

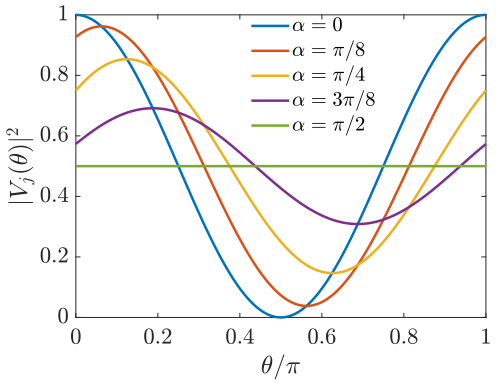

Fig. 12. Angular dependence of the intensity for all modes and several values of α.

The radial dependence of a few low-order modes is shown in Fig. 13. It can be observed that the highest amplitude is obtained for the first order mode. Moreover, the amplitude peak decreases monotonically for increasing mode order, with $n \geqslant 1$.

The combined effect of the radial and angular dependence (of the intensity) for the particular choice of $\alpha = \pi/4$ and $n = 5$ is shown as a color map in Fig. 14. The polarization pattern for this particular choice of $\alpha = \pi/4$ and two different values of β are superimposed to the intensity of such a mode.

The pseudo-modal expansion in Eq. (46) gives us some hints for

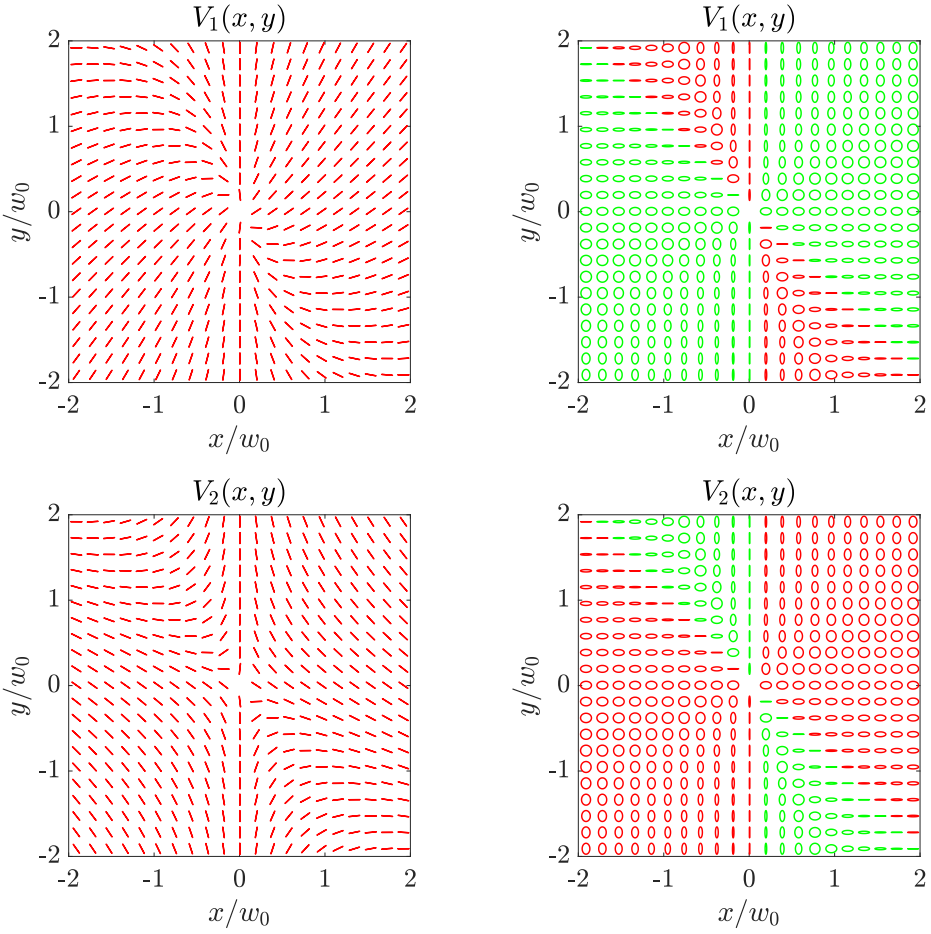

Fig. 11. Polarization maps for $\mathbf{V}_1(\theta)$ and $\mathbf{V}_2(\theta)$ across the source plane for $\alpha = \pi/4$ and $\beta = 0$(left column) and $\beta = \pi/2$(right column).

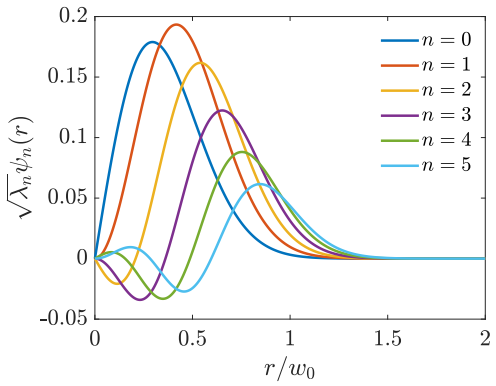

Fig. 13. Radial dependence of several modes.

possible synthesis procedures.

In the first scheme, whose working principle is shown in Fig. 15, the mode $\mathbf{\Psi}_{nj}(\mathbf{r})$ is produced as follows. The beam emitted by a laser is split into two replicas having orthogonal linear polarizations (say, x and y) by means of the polarizing beam splitter PBS. The replica polarized along x (y) is sent onto the spatial light modulator SLM_x (SLM_y), which provides it with the spatial modulation (both in phase and amplitude) corresponding to the x (y) component of $\mathbf{\Psi}_{nj}$. The two replicas are eventually recombined to obtain the whole mode and imaged by means of the converging lens L onto the source plane S, where a camera can detect the intensity profile. The sequence of the modes is obtained changing the transmission function of the SLMs in such a way that, at any step, a different combination of the indices n (ranging from 0 to a maximum value N) and j (1 or 2) is realized. The sum over the modes is then performed assigning a different weight to each of the modes, for instance on setting the integration time of the camera as proportional to the values of $\lambda_n a_j$. Of course, a real optical system implemented in a lab will take account of the peculiarities of the used components. For instance, SLMs may work in reflection, or may be of the phase-only type, in which case holographic approaches can be used to produce the required field distributions.

The second scheme, sketched in Fig. 16, exploits the factorization of the CSD matrix in Eq. (20). Here, the mutually uncorrelated fields $\mathbf{V}_1(\theta)$ and $\mathbf{V}_2(\theta)$ are produced simultaneously by means of two different laser (operating at the same frequency), having powers proportional to a_1 and a_2, respectively. To synthesize $\mathbf{V}_1(\theta)$ and $\mathbf{V}_2(\theta)$ starting from a linear polarization, the use of suitable polarization converters (PC_1 and PC_2) is required, but we will return to the subject shortly. The two fields are

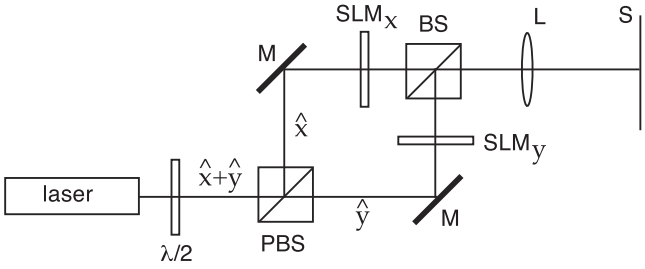

Fig. 15. Experimental set up for first approach.

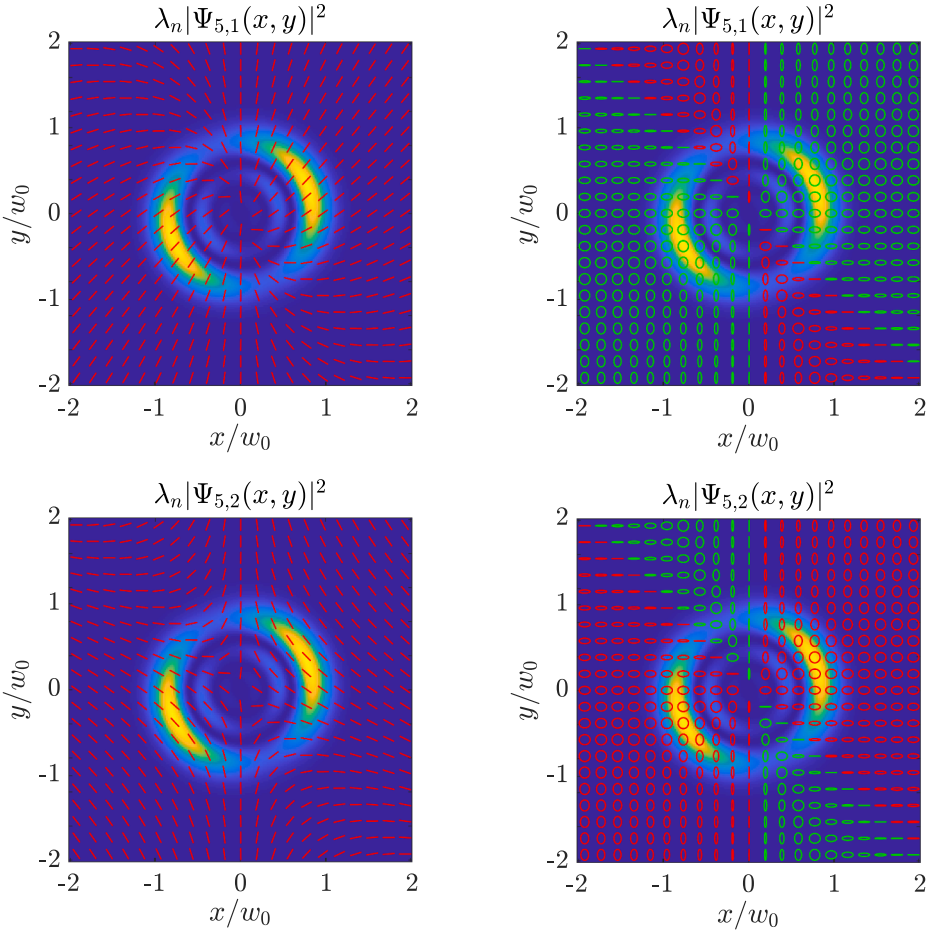

Fig. 14. Polariazation patterns for $\mathbf{V}_1(\theta)$ (top row) and $\mathbf{V}_2(\theta)$ (bottom row) with $\alpha=\pi/4$ for $\beta=0$ (left column) and $\beta=\pi/2$ (right column). These polarization maps are superimposed to the fith order radial mode.

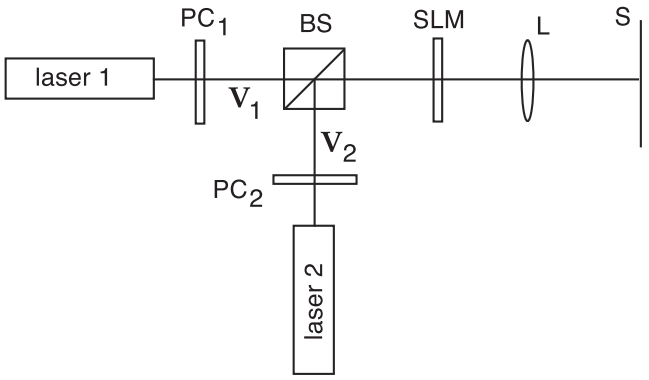

Fig. 16. Experimental set up for second approach.

then superimposed by means of a polarization-preserving beam splitter (BS). This corresponds to directly performing the sum over j in the expansion in Eq. (46). In other terms, the BCP matrix of the field exiting BS is just the one given by Eq. (43). Finally, the radial part of the CSD matrix is synthesized on letting the field exiting BS pass through a SLM, which provides it with the radial modulation $\psi_n(r)$. In conclusion, for any fixed value of the index n the field imaged onto the source plane has the CSD matrix given by

$$\widehat{W}_n(\mathbf{r}_1,\mathbf{r}_2) = \psi_n(r_1)\widehat{\Theta}(\theta_1,\theta_2)\psi_n(r_2). \tag{49}$$

Again, the sum over n can be performed integrating on the response time of the camera, which can be set according to the values of λ_n.

The advantage of the first scheme is that it is extremely general and can be adopted for the synthesis of any CSD matrix. It requires only one laser but two SLMs, and the number of modes to be presented in sequence is $2N$. In the second approach, the use of two lasers makes the synthesis process faster (the number of consecutive modes is N) and only one SLM is required. On the other hand, it may be difficult, in general, to physically realize such optical elements as PC_1 and PC_2 (if not through combinations of anisotroopic optical elements and SLMs). A significant exception occurs, however, when the polarization patterns to be synthesized have axial symmetry (such as radial, azimuthal or, more generally, spiral), in which case the polarization conversion can be obtained in a rather easy way starting from liquid cristal devices [19,75] or from glass windows under static stress [70].

7. Conclusions

In summary, a new class of partially coherent, partially and non-uniformly polarized sources of the pseudo-Schell model type is proposed and analyzed in detail. For these sources, not only does the polarization state change but the degree of polarization can change across the source plane from fully polarized to fully unpolarized. In either case, both the pattern of the polarization state and the degree of polarization remain unchanged during propagation. On the other hand, both the intensity profile and the coherence characteristics depend on the chosen source parameters. In general, both intensity and coherence change during propagation. In any case, the intensity, which in general does not have circular symmetry, always presents a null at the center of the source, which is conserved in the propagated beam. This results in a dark hollow beam with structured coherence and polarization. As in the scalar case, these beams also exhibit a self-focusing effect. The principal axes of the intensity distribution also remain invariant. In addition, both the electromagnetic DoC and the maximum-visibility DoC, measured over a ring concentric to the source, remain invariant in propagation. The above properties could be very useful in applications such as particle trapping, free space communications, etc. Finally, some experimental setups have been proposed to synthesize the proposed sources.

Declaration of Competing Interest

The authors declare that they have no known competing financial interests or personal relationships that could have appeared to influence the work reported in this paper.

Acknowledgements

This work has been supported by Spanish Ministerio de Economía y Competitividad under project PID2019 104268GB-C21.

References

[1] F. Wang, Y. Cai, Experimental generation of a partially coherent flat-topped beam, Opt. Lett. 33 (16) (2008) 1795–1797, https://doi.org/10.1364/OL.33.001795, http://ol.osa.org/abstract.cfm?URI=ol-33-16-1795.
[2] H. Lajunen, T. Saastamoinen, Propagation characteristics of partially coherent beams with spatially varying correlations, Opt. Lett. 36 (20) (2011) 4104–4106, https://doi.org/10.1364/OL.36.004104, http://ol.osa.org/abstract.cfm?URI=ol-36-20-4104.
[3] X. Li, F. Wang, Y. Cai, An alternative model for a partially coherent elliptical dark hollow beam, Opt. Laser Technol. 43 (3) (2011) 577–585, https://doi.org/10.1016/j.optlastec.2010.08.004, https://www.sciencedirect.com/science/article/pii/S0030399210002124.
[4] Y. Cai, Y. Chen, F. Wang, Generation and propagation of partially coherent beams with nonconventional correlation functions: a review [invited], J. Opt. Soc. Am. A 31 (9) (2014) 2083–2096, https://doi.org/10.1364/JOSAA.31.002083, http://josaa.osa.org/abstract.cfm?URI=josaa-31-9-2083.
[5] B. Rodenburg, M. Mirhosseini, O.S. Magaña-Loaiza, R.W. Boyd, Experimental generation of an optical field with arbitrary spatial coherence properties, J. Opt. Soc. Am. B 31 (6) (2014) A51–A55, https://doi.org/10.1364/JOSAB.31.000A51, http://josab.osa.org/abstract.cfm?URI=josab-31-6-A51.
[6] Y. Chen, S.A. Ponomarenko, Y. Cai, Experimental generation of optical coherence lattices, Appl. Phys. Lett. 109 (6) (2016) 061107, https://doi.org/10.1063/1.4960966, arXiv:https://doi.org/10.1063/1.4960966.
[7] M.W. Hyde IV, S.R. Bose-Pillai, R.A. Wood, Synthesis of non-uniformly correlated partially coherent sources using a deformable mirror, Appl. Phys. Lett. 111 (10) (2017) 101106, https://doi.org/10.1063/1.4994669.
[8] Y. Cai, Y. Chen, J. Yu, X. Liu, L. Liu, Generation of partially coherent beams, Progress Opt. 62 (2017) 157–223, https://doi.org/10.1016/bs.po.2016.11.001, http://www.sciencedirect.com/science/article/pii/S0079663816300166.
[9] M. Santarsiero, R. Martínez-Herrero, D. Maluenda, J.C.G. de Sande, G. Piquero, F. Gori, Partially coherent sources with circular coherence, Opt. Lett. 42 (8) (2017) 1512–1515, https://doi.org/10.1364/OL.42.001512, http://ol.osa.org/abstract.cfm?URI=ol-42-8-1512.
[10] M. Santarsiero, R. Martínez-Herrero, D. Maluenda, J.C.G. de Sande, G. Piquero, F. Gori, Synthesis of circularly coherent sources, Opt. Lett. 42 (20) (2017) 4115–4118, https://doi.org/10.1364/OL.42.004115, http://ol.osa.org/abstract.cfm?URI=ol-42-20-4115.
[11] X. Chen, J. Li, S.M.H. Rafsanjani, O. Korotkova, Synthesis of I_m-Bessel correlated beams via coherent modes, Opt. Lett. 43 (15) (2018) 3590–3593, https://doi.org/10.1364/OL.43.003590, http://ol.osa.org/abstract.cfm?URI=ol-43-15-3590.
[12] G. Piquero, M. Santarsiero, R. Martínez-Herrero, J.C.G. de Sande, M. Alonzo, F. Gori, Partially coherent sources with radial coherence, Opt. Lett. 43 (10) (2018) 2376–2379, https://doi.org/10.1364/OL.43.002376, http://ol.osa.org/abstract.cfm?URI=ol-43-10-2376.
[13] J.C.G. de Sande, R. Martínez-Herrero, G. Piquero, M. Santarsiero, F. Gori, Pseudo-Schell model sources, Opt. Express 27 (4) (2019) 3963–3977, https://doi.org/10.1364/OE.27.003963, http://www.opticsexpress.org/abstract.cfm?URI=oe-27-4-3963.
[14] R. Martínez-Herrero, G. Piquero, J.C.G. de Sande, M. Santarsiero, F. Gori, Besinc pseudo-Schell model sources with circular coherence, Appl. Sci. 9 (13) (2019), https://doi.org/10.3390/app9132716 https://www.mdpi.com/2076-3417/9/13/2716.
[15] M. Santarsiero, R. Martínez-Herrero, G. Piquero, J.C.G. de Sande, F. Gori, Modal analysis of pseudo-Schell model sources, Photonics 8 (10) (2021), https://doi.org/10.3390/photonics8100449 https://www.mdpi.com/2304-6732/8/10/449.
[16] O. Korotkova, F. Gori, Introduction to the special issue on structured light coherence, Photonics 8 (10) (2021), https://doi.org/10.3390/photonics8100457 https://www.mdpi.com/2304-6732/8/10/457.
[17] R. Martínez-Herrero, M. Santarsiero, G. Piquero, J.C. González de Sande, A new type of shape-invariant beams with structured coherence: Laguerre-Christoffel-Darboux beams, Photonics 8 (4) (2021), https://doi.org/10.3390/photonics8040134 https://www.mdpi.com/2304-6732/8/4/134.
[18] J. Tervo, Azimuthal polarization and partial coherence, J. Opt. Soc. Am. A 20 (10) (2003) 1974–1980, https://doi.org/10.1364/JOSAA.20.001974, http://josaa.osa.org/abstract.cfm?URI=josaa-20-10-1974.
[19] V. Ramírez-Sánchez, G. Piquero, M. Santarsiero, Synthesis and characterization of partially coherent beams with propagation-invariant transverse polarization pattern, Opt. Commun. 283 (22) (2010) 4484–4489, https://doi.org/10.1016/j.optcom.2010.04.081, http://www.sciencedirect.com/science/article/pii/S0030401810004220.

[20] M. Santarsiero, V. Ramírez-Sánchez, R. Borghi, Partially correlated thin annular sources: the vectorial case, J. Opt. Soc. Am. A 27 (6) (2010) 1450–1456, https://doi.org/10.1364/JOSAA.27.001450, http://josaa.osa.org/abstract.cfm?URI=josaa-27-6-1450.

[21] L. Guo, Z. Tang, C. Liang, Z. Tan, Intensity and spatial correlation properties of tightly focused partially coherent radially polarized vortex beams, Opt. Laser Technol. 43 (4) (2011) 895–898, https://doi.org/10.1016/j.optlastec.2010.10.002, https://www.sciencedirect.com/science/article/pii/S0030399210002446.

[22] Y. Chen, F. Wang, L. Liu, C. Zhao, Y. Cai, O. Korotkova, Generation and propagation of a partially coherent vector beam with special correlation functions, Phys. Rev. A 89 (2014) 013801, https://doi.org/10.1103/PhysRevA.89.013801, http://link.aps.org/doi/10.1103/PhysRevA.89.013801.

[23] R. Martínez-Herrero, D. Maluenda, G. Piquero, J.C.G. de Sande, M. Santarsiero, F. Gori, Partially polarized pseudo-Schell model sources, in: M.F.P.C.M.M. Costa (Ed.), Third International Conference on Applications of Optics and Photonics, vol. 10453, International Society for Optics and Photonics, SPIE, 2017, pp. 398–403, https://doi.org/10.1117/12.2272154.

[24] H.-F. Xu, Y. Zhou, H.-W. Wu, H.-J. Chen, Z.-Q. Sheng, J. Qu, Focus shaping of the radially polarized Laguerre-Gaussian-correlated Schell-model vortex beams, Opt. Express 26 (16) (2018) 20076–20088, https://doi.org/10.1364/OE.26.020076, http://www.osapublishing.org/oe/abstract.cfm?URI=oe-26-16-20076.

[25] M. Senthilkumar, K. Rajesh, M. Udhayakumar, Z. Jaroszewicz, G. Mahadevan, Focusing properties of spirally polarized sinh Gaussian beam, Opt. Laser Technol. 111 (2019) 623–628, https://doi.org/10.1016/j.optlastec.2018.10.048, https://www.sciencedirect.com/science/article/pii/S0030399218312738.

[26] M.W. Hyde, X. Xiao, D.G. Voelz, Generating electromagnetic nonuniformly correlated beams, Opt. Lett. 44 (23) (2019) 5719–5722, https://doi.org/10.1364/OL.44.005719, http://www.osapublishing.org/ol/abstract.cfm?URI=ol-44-23-5719.

[27] J. Yu, X. Zhu, S. Lin, F. Wang, G. Gbur, Y. Cai, Vector partially coherent beams with prescribed non-uniform correlation structure, Opt. Lett. 45 (13) (2020) 3824–3827, https://doi.org/10.1364/OL.397316, http://www.osapublishing.org/ol/abstract.cfm?URI=ol-45-13-3824.

[28] M.W. Hyde IV, Synthesizing general electromagnetic partially coherent sources from random, correlated complex screens, Optics 1 (1) (2020) 97–113, https://doi.org/10.3390/opt1010008, https://www.mdpi.com/2673-3269/1/1/8.

[29] R. Tong, Z. Dong, Y. Chen, F. Wang, Y. Cai, T. Setälä, Fast calculation of tightly focused random electromagnetic beams: controlling the focal field by spatial coherence, Opt. Express 28 (7) (2020) 9713–9727, https://doi.org/10.1364/OE.386187, http://www.osapublishing.org/oe/abstract.cfm?URI=oe-28-7-9713.

[30] X. Zhu, J. Yu, F. Wang, Y. Chen, Y. Cai, O. Korotkova, Synthesis of vector nonuniformly correlated light beams by a single digital mirror device, Opt. Lett. 46 (12) (2021) 2996–2999, https://doi.org/10.1364/OL.428508, http://www.osapublishing.org/ol/abstract.cfm?URI=ol-46-12-2996.

[31] J.C. Ricklin, F.M. Davidson, Atmospheric turbulence effects on a partially coherent Gaussian beam: implications for free-space laser communication, J. Opt. Soc. Am. A 19 (9) (2002) 1794–1802, https://doi.org/10.1364/JOSAA.19.001794, http://josaa.osa.org/abstract.cfm?URI=josaa-19-9-1794.

[32] O. Korotkova, L.C. Andrews, R.L. Phillips, Model for a partially coherent Gaussian beam in atmospheric turbulence with application in Lasercom, Opt. Eng. 43 (2) (2004) 330–341, https://doi.org/10.1117/1.1636185.

[33] S.B. Raghunathan, T. van Dijk, E.J.G. Peterman, T.D. Visser, Experimental demonstration of an intensity minimum at the focus of a laser beam created by spatial coherence: application to the optical trapping of dielectric particles, Opt. Lett. 35 (24) (2010) 4166–4168, https://doi.org/10.1364/OL.35.004166, http://ol.osa.org/abstract.cfm?URI=ol-35-24-4166.

[34] C. Zhao, Y. Cai, Trapping two types of particles using a focused partially coherent elegant Laguerre-Gaussian beam, Opt. Lett. 36 (12) (2011) 2251–2253, https://doi.org/10.1364/OL.36.002251, http://ol.osa.org/abstract.cfm?URI=ol-36-12-2251.

[35] G. Wu, Y. Cai, Detection of a semirough target in turbulent atmosphere by a partially coherent beam, Opt. Lett. 36 (10) (2011) 1939–1941, https://doi.org/10.1364/OL.36.001939, http://ol.osa.org/abstract.cfm?URI=ol-36-10-1939.

[36] X. Liu, Y. Shen, L. Liu, F. Wang, Y. Cai, Experimental demonstration of vortex phase-induced reduction in scintillation of a partially coherent beam, Opt. Lett. 38 (24) (2013) 5323–5326, https://doi.org/10.1364/OL.38.005323, http://www.osapublishing.org/ol/abstract.cfm?URI=ol-38-24-5323.

[37] G. Gbur, Partially coherent beam propagation in atmospheric turbulence [invited], J. Opt. Soc. Am. A 31 (9) (2014) 2038–2045, https://doi.org/10.1364/JOSAA.31.002038, http://josaa.osa.org/abstract.cfm?URI=josaa-31-9-2038.

[38] H. Wang, H. Wang, Y. Xu, X. Qian, Intensity and polarization properties of the partially coherent Laguerre-Gaussian vector beams with vortices propagating through turbulent atmosphere, Opt. Laser Technol. 56 (2014) 1–6, https://doi.org/10.1016/j.optlastec.2013.06.026, https://www.sciencedirect.com/science/article/pii/S0030399213002429.

[39] C. Ding, M. Koivurova, J. Turunen, L. Pan, Self-focusing of a partially coherent beam with circular coherence, J. Opt. Soc. Am. A 34 (8) (2017) 1441–1447, https://doi.org/10.1364/JOSAA.34.001441, http://josaa.osa.org/abstract.cfm?URI=josaa-34-8-1441.

[40] H. Zhang, J. Li, K. Cheng, M. Duan, Z. Feng, Trapping two types of particles using a focused partially coherent circular edge dislocations beam, Opt. Laser Technol. 97 (2017) 191–197, https://doi.org/10.1016/j.optlastec.2017.06.025, http://www.sciencedirect.com/science/article/pii/S0030399217301561.

[41] D. Wu, F. Wang, Y. Cai, High-order nonuniformly correlated beams, Opt. Laser Technol. 99 (2018) 230–237, https://doi.org/10.1016/j.optlastec.2017.09.007, http://www.sciencedirect.com/science/article/pii/S0030399217304553.

[42] A. Bhattacharjee, A.K. Jha, Experimental demonstration of structural robustness of spatially partially coherent fields in turbulence, Opt. Lett. 45 (14) (2020) 4068–4071, https://doi.org/10.1364/OL.395697, http://www.osapublishing.org/ol/abstract.cfm?URI=ol-45-14-4068.

[43] Y. Shen, H. Sun, D. Peng, Y. Chen, Q. Cai, D. Wu, F. Wang, Y. Cai, S. A. Ponomarenko, Optical image reconstruction in 4f imaging system: Role of spatial coherence structure engineering, Appl. Phys. Lett. 118 (18) (2021) 181102, https://doi.org/10.1063/5.0046288, arXiv:https://doi.org/10.1063/5.0046288.

[44] T. Eitoku, M. Tange, H. Kato, T. Okazaki, Depolarized dynamic light scattering study of multi-walled carbon nanotubes in solution, Mater. Express 3 (1) (2013) 37–42, https://doi.org/10.1166/mex.2013.1096, https://www.ingentaconnect.com/content/asp/me/2013/00000003/00000001/art00005.

[45] X. Ling, X. Zhou, X. Yi, Geometric spin Hall effect of light with inhomogeneous polarization, Opt. Commun. 383 (2017) 412–417, https://doi.org/10.1016/j.optcom.2016.09.043, https://www.sciencedirect.com/science/article/pii/S0030401816308264.

[46] J.C.G. de Sande, M. Santarsiero, G. Piquero, Spirally polarized beams for polarimetry measurements of deterministic and homogeneous samples, Opt. Lasers Eng. 91 (2017) 97–105, https://doi.org/10.1016/j.optlaseng.2016.11.008, http://www.sciencedirect.com/science/article/pii/S0143816616304171.

[47] J.C.G. de Sande, G. Piquero, J.C. Suárez-Bermejo, M. Santarsiero, Mueller matrix polarimetry with invariant polarization pattern beams, Photonics 8 (11) (2021), https://doi.org/10.3390/photonics8110491 https://www.mdpi.com/2304-6732/8/11/491.

[48] E. Wolf, Introduction to the Theory of Coherence and Polarization of Light, Cambridge University Press, 2007.

[49] F. Gori, M. Santarsiero, S. Vicalvi, R. Borghi, G. Guattari, Beam coherence-polarization matrix, Pure Appl. Opt.: J. Eur. Opt. Soc. Part A 7 (5) (1998) 941, http://stacks.iop.org/0963-9659/7/i=5/a=004.

[50] F. Gori, V. Ramírez-Sánchez, M. Santarsiero, T. Shirai, On genuine cross-spectral density matrices, J. Opt. A: Pure Appl. Opt. 11 (8) (2009) 085706, http://stacks.iop.org/1464-4258/11/i=8/a=085706.

[51] R. Martínez-Herrero, P.M. Mejías, Elementary-field expansions of genuine cross-spectral density matrices, Opt. Lett. 34 (15) (2009) 2303–2305, https://doi.org/10.1364/OL.34.002303, http://ol.osa.org/abstract.cfm?URI=ol-34-15-2303.

[52] D.H. Goldstein, Polarized Light, second (revised and expanded) Edition, Marcel Dekker Inc, 2003.

[53] L. Mandel, E. Wolf, Optical Coherence and Quantum Optics, Cambridge University Press, 1995, https://doi.org/10.1017/CBO9781139644105.

[54] J. Tervo, T. Setälä, A.T. Friberg, Degree of coherence for electromagnetic fields, Opt. Express 11 (10) (2003) 1137–1143, https://doi.org/10.1364/OE.11.001137, http://www.opticsexpress.org/abstract.cfm?URI=oe-11-10-1137.

[55] T. Setälä, J. Tervo, A.T. Friberg, Complete electromagnetic coherence in the space–frequency domain, Opt. Lett. 29 (4) (2004) 328–330, https://doi.org/10.1364/OL.29.000328, http://ol.osa.org/abstract.cfm?URI=ol-29-4-328.

[56] F. Gori, M. Santarsiero, R. Borghi, Maximizing Young's fringe visibility through reversible optical transformations, Opt. Lett. 32 (6) (2007) 588–590, https://doi.org/10.1364/OL.32.000588, http://ol.osa.org/abstract.cfm?URI=ol-32-6-588.

[57] R. Martínez-Herrero, P.M. Mejías, Maximum visibility under unitary transformations in two-pinhole interference for electromagnetic fields, Opt. Lett. 32 (11) (2007) 1471–1473, https://doi.org/10.1364/OL.32.001471, http://ol.osa.org/abstract.cfm?URI=ol-32-11-1471.

[58] A. Luis, Degree of coherence for vectorial electromagnetic fields as the distance between correlation matrices, J. Opt. Soc. Am. A 24 (4) (2007) 1063–1068, https://doi.org/10.1364/JOSAA.24.001063, http://josaa.osa.org/abstract.cfm?URI=josaa-24-4-1063.

[59] E. Wolf, Unified theory of coherence and polarization of random electromagnetic beams, Phys. Lett. A 312 (5) (2003) 263–267, https://doi.org/10.1016/S0375-9601(03)00684-4, https://www.sciencedirect.com/science/article/pii/S0375960103006844.

[60] S.A. Ponomarenko, E. Wolf, The spectral degree of coherence of fully spatially coherent electromagnetic beams, Opt. Commun. 227 (1) (2003) 73–74, https://doi.org/10.1016/j.optcom.2003.09.047, https://www.sciencedirect.com/science/article/pii/S0030401803019709.

[61] M. Alonzo, M. Santarsiero, F. Gori, Maximizing Young fringe visibility with a universal SU2 polarization gadget, Opt. Lett. 43 (12) (2018) 2844–2847, https://doi.org/10.1364/OL.43.002844, http://ol.osa.org/abstract.cfm?URI=ol-43-12-2844.

[62] R. Simon, N. Mukunda, Universal SU(2) gadget for polarization optics, Phys. Lett. A 138 (9) (1989) 474–480, https://doi.org/10.1016/0375-9601(89)90748-2, http://www.sciencedirect.com/science/article/pii/0375960189907482.

[63] R. Martínez-Herrero, P.M. Mejías, Relation between degrees of coherence for electromagnetic fields, Opt. Lett. 32 (11) (2007) 1504–1506, https://doi.org/10.1364/OL.32.001504, http://ol.osa.org/abstract.cfm?URI=ol-32-11-1504.

[64] J. Serna, P. Mejías, R. Martínez-Herrero, Rotation of partially coherent beams propagating through free space, Opt. Quant. Electron. 24 (9) (1992) S873–S880.

[65] R. Martínez-Herrero, P. Mejías, On the spatial orientation of the transverse irradiance profile of partially coherent beams, Opt. Express 14 (8) (2006) 3294–3303.

[66] M. Abramowitz, I. Stegun (Eds.), Handbook of Mathematical Functions, Dover Publications Inc, 1972.

[67] Y. Cai, X. Lu, Q. Lin, Hollow Gaussian beams and their propagation properties, Opt. Lett. 28 (13) (2003) 1084–1086, https://doi.org/10.1364/OL.28.001084, http://ol.osa.org/abstract.cfm?URI=ol-28-13-1084.
[68] X. Lü, Y. Cai, Partially coherent circular and elliptical dark hollow beams and their paraxial propagations, Phys. Lett. A 369 (1) (2007) 157–166, https://doi.org/10.1016/j.physleta.2007.04.065, http://www.sciencedirect.com/science/article/pii/S0375960107006329.
[69] L.-G. Wang, L.-Q. Wang, Hollow Gaussian Schell-model beam and its propagation, Opt. Commun. 281 (6) (2008) 1337–1342, https://doi.org/10.1016/j.optcom.2007.11.018, http://www.sciencedirect.com/science/article/pii/S003040180701190X.
[70] A.M. Beckley, T.G. Brown, M.A. Alonso, Full Poincaré beams ii: partial polarization, Opt. Express 20 (9) (2012) 9357–9362, https://doi.org/10.1364/OE.20.009357, http://www.opticsexpress.org/abstract.cfm?URI=oe-20-9-9357.
[71] R. Wang, S. Zhu, Y. Chen, H. Huang, Z. Li, Y. Cai, Experimental synthesis of partially coherent sources, Opt. Lett. 45 (7) (2020) 1874–1877, https://doi.org/10.1364/OL.388307, http://ol.osa.org/abstract.cfm?URI=ol-45-7-1874.
[72] S. Zhu, P. Li, Z. Li, Y. Cai, W. He, Generating non-uniformly correlated twisted sources, Opt. Lett. 46 (20) (2021) 5100–5103, https://doi.org/10.1364/OL.442264, http://www.osapublishing.org/ol/abstract.cfm?URI=ol-46-20-5100.
[73] F. Gori, M. Santarsiero, R. Simon, G. Piquero, R. Borghi, G. Guattari, Coherent-mode decomposition of partially polarized, partially coherent sources, J. Opt. Soc. Am. A 20 (1) (2003) 78–84, https://doi.org/10.1364/JOSAA.20.000078, http://josaa.osa.org/abstract.cfm?URI=josaa-20-1-78.
[74] R. Martínez-Herrero, P.M. Mejías, F. Gori, Genuine cross-spectral densities and pseudo-modal expansions, Opt. Lett. 34 (9) (2009) 1399–1401, https://doi.org/10.1364/OL.34.001399, http://ol.osa.org/abstract.cfm?URI=ol-34-9-1399.
[75] G. Piquero, R. Martínez-Herrero, J.C.G. de Sande, M. Santarsiero, Synthesis and characterization of non-uniformly totally polarized light beams: tutorial, J. Opt. Soc. Am. A 37 (4)(ts) (2020) 591–605. https://doi.org/10.1364/JOSAA.379439. http://josaa.osa.org/abstract.cfm?URI=josaa-37-4-591.